Biophysical Journal
Article

Biophysical Society

Protein Motion and Configurations in a Form-Fitting Nanopore: Avidin in ClyA

Bo Lu,[1] Chris Stokes,[2] Monifa Fahie,[3] Min Chen,[3] Jene A. Golovchenko,[1,4] and Lene Vestergaard Hau[1,4,*]
[1]Department of Physics, Harvard University, Cambridge, Massachusetts; [2]The Rowland Institute at Harvard, Harvard University, Cambridge, Massachusetts; [3]Department of Chemistry, University of Massachusetts, Amherst, Massachusetts; and [4]School of Engineering and Applied Sciences, Harvard University, Cambridge, Massachusetts

ABSTRACT We probe the molecular dynamics and states of an avidin protein as it is captured and trapped in a voltage-biased cytolysin A nanopore using time-resolved single-molecule electrical conductance signals. The data for very large numbers of single-molecule events are analyzed and presented by a new method that provides clear visual insight into the molecular scale processes. Avidin in cytolysin A has surprisingly rich conductance spectra that reveal transient and more permanently trapped protein configurations in the pore and how they evolve into one another. We identify a long-lasting, stable, and low-noise configuration of avidin in the nanopore into which avidin can be reliably trapped and released. This may prove useful for single-molecule studies of other proteins that can be biotinylated and then transported by avidin to the pore via their coupling to avidin with biotin-avidin linking. We demonstrate the sensitivity of this system with detection of biotin attached to avidin captured by the pore.

INTRODUCTION

It is possible to observe individual charged biological molecules as they translocate through a voltage-biased nanopore in a lipid membrane by monitoring the ionic conductance of the pore during the molecular motion through the pore. Such measurements have provided new insights into the biophysics of these molecules and their interactions with the pores (1). They have also resulted in practical, portable instruments for sequencing DNA (https://nanoporetech.com/). Probing proteins by this translocation method has provided interesting insights but proved challenging due to the more complex geometrical and charge structures of proteins; however, progress is being made (2–7).

We use an alternative method that involves studying proteins that do not pass through the pore but are rather transiently or more permanently trapped within a large pore by electrophoretic attraction. The method has been pursued recently (8,9) in cytolysin A (ClyA) nanopores and shown great promise. In the following, we show that when a very close match between the protein size and the pore lumen size is chosen, remarkably detailed, time-dependent electrical-conductance spectra are observed that reveal discrete protein configurations with the pore, including a low-noise and long-lasting trapped state that can be cleared deterministically with a control voltage.

The size-matched pair we have chosen is avidin in $ClyA_{12}$, a dodecamer nanopore, because the molecular structures suggest the possibility of at least one highly constrained geometrical configuration (which we observe). Avidin is a positively charged protein with a high isoelectric point of roughly 10 (10,11), and its size is well understood from x-ray studies (12,13). The ClyA pore exists in several oligomeric forms, each having a different pore size and open-pore conductance, but the dodecamer pore is the most stable (14,15).

We also present, what is to our knowledge, a new method for analyzing and visualizing the data for very large numbers of single molecule events of protein trapping in a nanopore. The method provides clear views of the global dynamics and reveals molecular scale configurations and their evolution, even for relatively rare short events.

Finally, we demonstrate the sensitivity of the avidin $ClyA_{12}$ system to molecular perturbations by detecting biotin linked to the avidin protein in the deeply trapped state.

MATERIALS AND METHODS

The protein-nanopore system

Fig. 1 *A* shows molecular models, with dimensions, of the avidin and dodecamer $ClyA_{12}$ nanopore. The close match between the avidin outer dimensions and the pore lumen's inner dimension makes this pair

Submitted January 18, 2018, and accepted for publication July 25, 2018.
*Correspondence: hau@g.harvard.edu
Editor: Antoine van Oijen.
https://doi.org/10.1016/j.bpj.2018.07.024

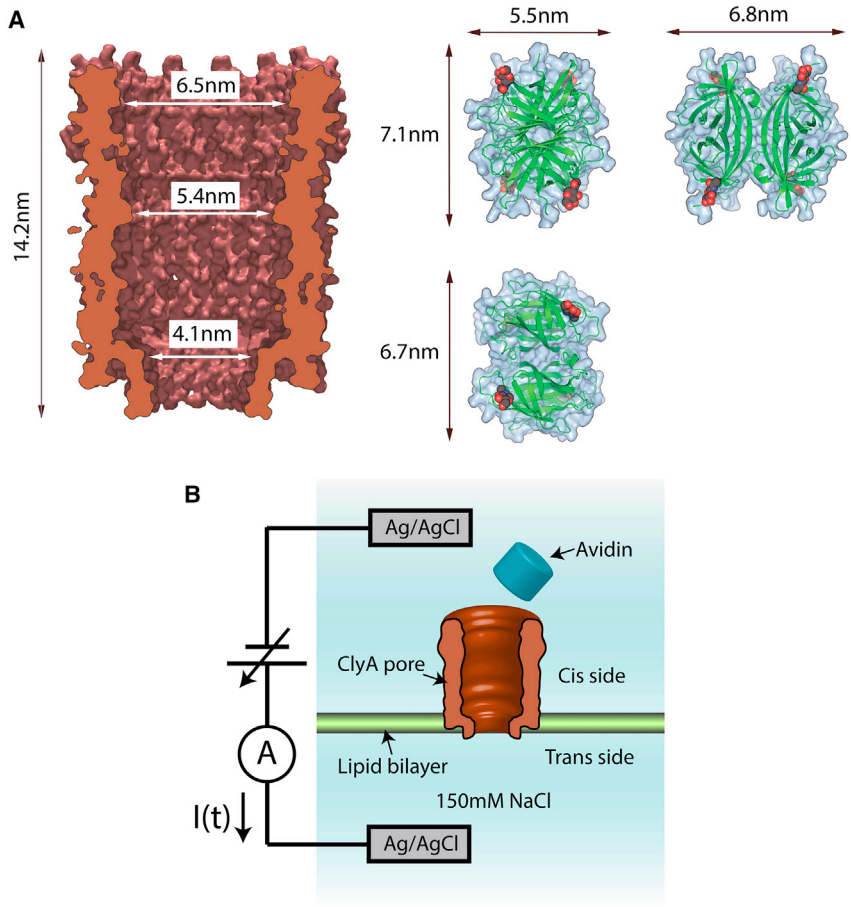

FIGURE 1 Avidin-ClyA setup. (*A*) Protein structures of the ClyA dodecamer pore and of avidin. The figures are based on the x-ray crystallography structures 2WCD and 1AVE, respectively, from the Protein Database. The ClyA pore is shown in a cross-sectional view along the center plane containing the 12-fold rotational symmetry axis. Avidin is viewed from three different, orthogonal directions. Two of its four β barrels are visible in the figures (*green*) as are two of the four N-Acetylglucosamines (oxygens are *red*). (*B*) The experimental setup is shown. A lipid bilayer membrane is suspended across a 40 μm teflon frame in an electrolytic buffer solution (150 mM NaCl, 15 mM Tris pH 7.5). A silver/silver-chloride electrode is placed in each reservoir, and a voltage of a few tens of mV, typically, is applied across the membrane. The membrane electrically isolates the two reservoirs, and initially no current flows between the electrodes. Preformed ClyA pores are added to the *cis* side, and when a single pore inserts in the membrane—observed as a step change in current to a stable open-pore current—the *cis* side is immediately flushed with buffer electrolyte solution to prevent additional ClyA pores from inserting. Once a single pore is in place in the membrane, 10 pmol of avidin is added to the *cis* chamber. With a negative bias voltage applied, the current is transiently blocked when individual, positively charged avidin molecules are trapped by and subsequently escape or, by voltage reversal, are ejected from the pore.

attractive for our purposes. These models and dimensions have been determined by x-ray diffraction (12,13,15) and can be found in the protein database (16).

ClyA is a pore forming cytolytic toxin expressed in several pathogenic strains of *Escherichia coli* and *Salmonella enterica*. Upon reaching a target-cell membrane, the soluble 34 kilodaltons (kDa) ClyA monomers undergo significant conformational changes, involving half of the monomers' amino acid residues, and subsequently assemble into membrane-bound oligomers (15,17). The resulting membrane-spanning ClyA pores form nanometer-sized circular holes in the membrane whose function as a cell barrier is lost, and this ultimately leads to cell death. It is clear from multiple observed pore conductances and gel studies that different oligomers of ClyA exist and may be of use for other protein nanopore studies (14).

Commercially available avidin (Pierce Avidin; Thermo Fisher Scientific, Waltham, MA) is purified from hen egg white, and the molecule is a tetramer that consists of four β barrels. Each barrel is open at one end, which allows one end of its ligand biotin to enter and bind to residues inside the β barrel (12,13). (In Fig. 1 *A*, two of the β barrels (*green*) are clearly visible.) The binding of biotin to avidin represents the strongest noncovalent ligand bond found in nature (with a dissociation constant of 10^{-15} M), and the protein-ligand pair has been used extensively in molecular biology, biotechnology, and medical applications (18). In our experiments, we first use apo-avidin (with no biotin bound). Avidin is a glyco-protein with one asparagine glycosylation binding site per monomer (Asn17). A single core N-Acetylglucosamine (GlcNAc) is visible at two sites in the image, which is based on the crystal structure 1AVE in the protein database (16). This structure has a charge of roughly seven positive charges at the pH of 7.5 used in the experiments in this article (19).

Avidin used in our experiments (Pierce Avidin; Thermo Fisher Scientific) has a polysaccharide attached to each of the four Asn17 locations. In addition to the core GlcNAc, the polysaccharides have four to five mannose and 2 GlcNAc (11).

Experimental setup

Fig. 1 *B* illustrates the experimental setup. Two chambers of electrolyte solution (150 mM NaCl, 15 mM Tris at pH 7.5) are separated and electrically isolated from each other by a lipid bilayer of 1,2-diphytanoyl-*sn*-glycero-3-phosphocholine (Avanti Polar Lipids, Alabaster, AL) stretched across a 40-micron diameter teflon frame. Ag/AgCl electrodes are inserted in each chamber and a voltage bias is applied across the membrane. For later trapping of positively charged avidin in the pore, the trans chamber is kept at negative voltage. ClyA nanopores are first added to the *cis* chamber. When a single pore inserts in the membrane, the ionic current induced by the voltage bias abruptly increases, after which the remaining nanopores in solution are removed (flushed) from the *cis* chamber.

The current observed for individual voltage-biased nanopores is measured, and for the work reported here, nanopores with a conductance of 1.66 nS ($\pm$1%) at 30 mV bias were selected.

This conductance value is the most commonly observed in our experiments and is the only pore conductance that shows long-term stability (>5 min).

For all current measurements, we used a Molecular Devices (San Jose, CA) Axopatch 200B patch clamp amplifier. The output signal was processed by a 10 kHz, four pole Bessel filter to minimize high-frequency current noise. After filtering, the signal was sampled and digitized every 4 μs and recorded in computer memory for further processing and analysis.

ClyA monomer expression and purification

All reagents were purchased from Fisher Scientific and/or Boston Bioproducts (Ashland, MA) unless otherwise stated. Phenylmethane sulfonyl fluoride and magnesium chloride were purchased from Sigma (St. Louis, MO).

C-terminal His_6 tagged ClyAwt protein was expressed in BL21 (DE3) cells. Specifically, pT7-ClyAwt-$CHis_6$ plasmid was transformed in BL21 (DE3) chemically competent cells and grown on Luria-Bertani (LB)-Amp Agar plates. One colony was inoculated in starter LB media containing 100 μg/mL ampicillin antibiotic and grown at 37°C with shaking at 200 revolutions per minute. The starter culture was used to inoculate 250 mL LB media containing 100 μg/mL ampicillin. The culture was grown at 37°C until the OD_{600} was between 0.5 and 0.65. The culture was then cooled on ice and induced by adding isopropylthiogalactoside to a final concentration of 0.5 mM and then incubated for 16 h at 15°C with shaking. After 16 h, the culture was harvested at 3100 × *g* and the pellet resuspended in 15 mL of 50 mM Tris-HCl pH 8.0, 1 mM ethylenediaminetetraacetic-acid buffer and frozen in −20°C until ready to use.

The frozen pellet was subsequently thawed at room temperature and a final concentration of 0.5 mM phenylmethane sulfonyl fluoride was added. The mixture was sonicated on ice to lyse the cells. $MgCl_2$ was added to the lysate at a final concentration of 10 mM and the mixture was then centrifuged for 20 min at 20,000 × *g*. The supernatant was filtered through a 0.22 μm filter membrane and loaded onto a gravity nickel-nitrilotriacetic acid column equilibrated with buffer A (150 mM NaCl, 50 mM Tris-HCl pH 8). The column was subsequently washed with buffer A to remove unbound proteins. Buffer A1 (150 mM NaCl, 50 mM Tris-HCl, 50 mM imidazole) was used to wash the weakly bound proteins and then the ClyA protein was eluted and collected in buffer A2 (150 mM NaCl, 50 mM Tris-HCl, 150 mM imidazole).

The eluted ClyA proteins were dialyzed using a 6–8 kDa cutoff membrane with constant stirring at 4°C for two cycles in dialysis buffer (150 mM NaCl, 50 mM Tris-HCl, 5 mM ethylenediaminetetraacetic acid). The proteins were then concentrated using a 10 kDa cutoff centricon to ∼3 mL and loaded onto a gel filtration column equilibrated in 150 mM NaCl, 20 mM sodium phosphate pH 7.0 buffer to remove aggregated proteins. The ClyA monomer was collected and kept at 4°C for 2 weeks or in −80°C for long-term storage.

Preparation and purification of ClyA oligomers

Purified ClyA monomers were suspended at 0.6 mg/ml in a buffered solution containing 50 mM NaCl, 10 mM sodium phosphate pH 7.4 (with a buffer exchange column). Oligomeric ClyA was formed from monomers by the addition of n-Dodecyl β-D- maltoside (10% w/v in water; DDM, Calbiochem/EMD Millipore, Billerica, MA) to a final concentration of 1% and incubated 20 min at room temperature.

ClyA nanopore purification was carried out by blue native gel electrophoresis using a 4–16% polyacrylamide gradient gel (NativePAGE; Invitrogen/Novex Life Technologies, Carlsbad, CA). Typically, 10 μg of ClyA oligomers were combined with electrophoresis loading buffer and applied to a 1.0 × 5.0 mm sample well of the gel. Major bands of oligomeric ClyA were excised from the gel following electrophoresis, and nanopores were recovered from the gel slices by diffusion into an elution buffer containing 150 mM NaCl, 0.2% DDM, 50 mM Tris-HCl pH 8.0.

Preparation of avidin

Lyophilized purified avidin from hen egg white (Product# 21121; Pierce/Thermo Scientific) was dissolved in deionized water to 2 mg/mL concentration. For subsequent storage at 4°C, an equal volume of 2× Phosphate Buffered Saline with 20% glycerol was added to the suspension to bring the avidin stock solution concentration to a nominal 1 mg/mL. Before use in ClyA nanopore experiments, an aliquot of the avidin stock solution was applied to a Bio-Spin 30 spin column (Bio-Rad Laboratories, Hercules, CA) equilibrated with 150 mM NaCl, 15 mM Tris-HCl pH 7.5 for buffer exchange.

Preparation of d-biotin

Biotin was prepared with 0.2 mg d-Biotin (Sigma-Aldrich/Millipore Sigma) per mL of 20 mM KCl, 50 mM Tris-HCl pH 7.6, and diluted in 150 mM NaCl, 15 mM Tris-HCl pH 7.5 to a final biotin concentration of 100 μM.

RESULTS AND DISCUSSION

Avidin in a 1.66 nS pore

After 10 pmol of avidin is added to the 250 μL *cis* chamber with a 1.66 nS pore in place, the current through the −35 mV voltage-biased pore is observed to transiently drop from the open pore value (58 pA) as individual avidin protein molecules are captured by, and escape from, the pore (Fig. 2, *A–G*). These current blockage events are separated into two categories. The first we call transient captures. It consists of transient current blockage events that last from 200 μs up to 1 s before the pore current returns to the open-pore value after a captured protein has spontaneously escaped from the pore. The second category we call permanent captures. These events last for times exceeding 1 s, and the captured protein is almost never observed to spontaneously leave the pore. For these events, we automatically reverse voltage bias after 1 s of current blockage. This ejects the positively charged protein from the pore. The voltage bias is then returned to the original polarity (negative voltage on the trans electrode) and the open pore current is again observed, followed by new current blockage capture events. Thus, our permanent events all last for 1 s, at which time the trapped avidin is forcibly ejected from the pore.

Each single protein capture, whether transient or permanent, is observed to have its own unique time-dependent current trace during the event. Fig. 2, *A–G* show a collection of single molecule capture events in the 1.66 nS pore. We plot the observed current $I(t)$ during each event, divided by the open pore current I_0. The events in Fig. 2, *A–E* show the time-dependent blockage for transient events of increasing duration. Most transient events are simple, having only a single blockade level as in the first event in Fig. 2 *A*. The longer transient events, Fig. 2, *B–E*, have been chosen to show that sometimes transitions between levels are observed during a single event. In a first-pass analysis, each transient capture is characterized by two numbers: the duration and the average blockage during the event. The "blockage" is defined to be $(I_0-I(t))/I_0$ averaged over each event's duration. Fig. 2 *H* is a "scatter plot" of these parameters for each transient capture event (*green points*) reflecting this characterization. (Each *green point* belongs to one protein capture). Scatter plots for other bias voltages are shown in Fig. S1.

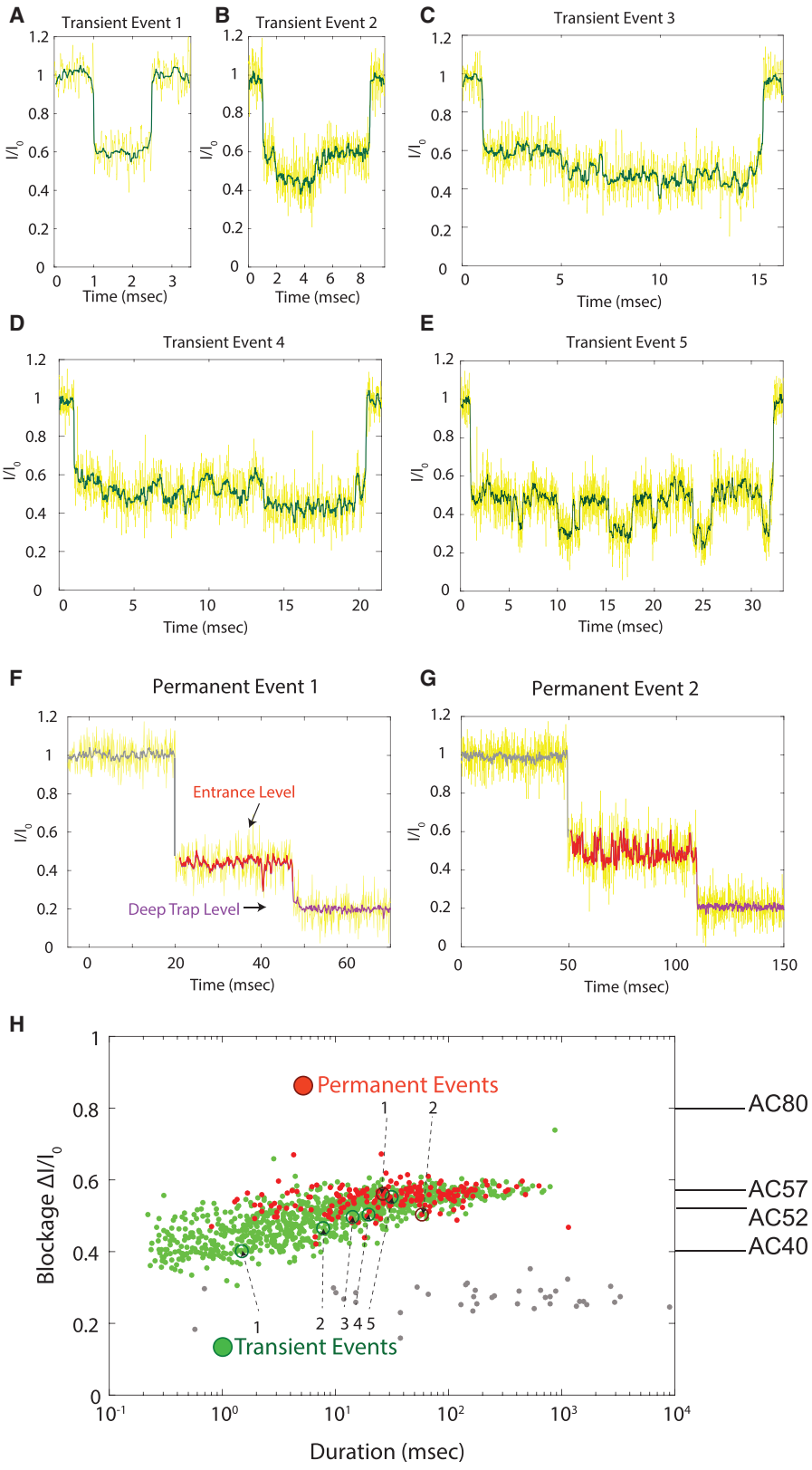

FIGURE 2 Capture events for individual avidin molecules. (*A–G*) Time traces for capture events are shown. We show both data points that were filtered with a 10 kHz four pole Bessel filter (*yellow*) and data that have been post-processed with a 1 kHz low-pass eight-pole Bessel filter (*red/maroon*). The first five (*A–E*) are transient events of increasing duration. Some have a rich time structure, with discrete blockage levels and transitions between them. The last two time traces (*F* and *G*) are for permanent events. Here, an immediate current drop to an entrance blockage level is followed by a transition to a deep, permanent capture level with very low current fluctuations. For all permanent events, we apply a +100 mV voltage pulse to eject the avidin from the pore after 1 s of trapping. (*H*). Scatter plot of event blockage versus duration. Each transient event, shown as a green dot in the figure, is characterized by its duration and average blockage. Each permanent event, represented by a red dot, is characterized by the time spent at the entrance level, and the corresponding average blockage, before transition into the permanent, deep blockage level, AC80. The seven events in (*A*)–(*G*) are indicated in the figure. We also mark the blockage levels AC40, AC52, and AC57 discussed in the text and visible in one or more of the time traces in (*A–G*).

As the transient capture event duration increases from a few hundred microseconds to a few hundred milliseconds, the average blockage slowly increases. In the next figure we will show that the reason for this is the existence of multiple discrete blockage levels that are averaged over in each event in the scatter plot. A few examples of separate and clearly distinguishable blockage levels and transitions between them are already seen in Fig. 2, *A–E*, and these events are also numbered in the scatter plot.

Fig. 2, *F* and *G* show the current traces for two permanent captures. Each of these events has an interesting time structure. As with most permanent capture events, they start with an intermediate, fluctuating blockage level that is followed by a deep and quiet permanent blockage level. The difference in low-frequency current-noise characteristics between the intermediate level and the permanent blockage level it leads to is seen clearly in the 1 kHz post-filtered time traces (*red/maroon data traces*) in Fig. 2, *F* and *G*. Quantitatively, for the full-bandwidth (10 kHz) data, the power spectral density for the permanent level is nearly constant at frequencies below 3 kHz with a (square root) value of 10 fA/root-Hz, whereas the power spectrum for the intermediate level exhibits a significant 1/f noise component. At 1 kHz, the current noise for the permanent trap level is 10 times smaller than the value for the intermediate level. It is also 20% smaller than that for the open pore, which in turn is within a factor of 2 of the Johnson noise limit.

Permanent captures are characterized by the time duration and average blockage during the intermediate part of the event. With these parameters, each permanent capture event is added to the scatter plot of Fig. 2 *H* (*red*). The average blockage is clearly independent of duration and close to that of the longest transient events. This immediately suggests that, before capture to a deep permanent trap state, the protein often passes through a particular intermediate state of variable duration. The permanent trap state may be of special importance for future protein studies as discussed below. The protein often stays trapped in this state even after the voltage bias has been removed but can always be cleared by a large reverse bias voltage.

Protein dynamics landscape analysis

A global view of these complex dynamical signals and the existence of discrete blockage levels and their time-dependent populations are revealed clearly and quantitatively in the protein dynamics landscape (PDL) analysis and plots that we introduce for the first time in connection with Fig. 3. To generate a particular histogram in Fig. 3 *A*, all transient events that last for times less than a specified τ_{trans} are pooled. Then the amount of time spent (in units of 160 μs time bins) at each blockage level for all these events is determined and a histogram of the time spent at each level is generated. We refer to this histogram as a blockage spectrum. A collection of such blockage spectra, for a set of increasing τ_{trans} values, is a PDL. Note that selecting data for small τ_{trans} allows rare, short events to be visualized and quantified accurately.

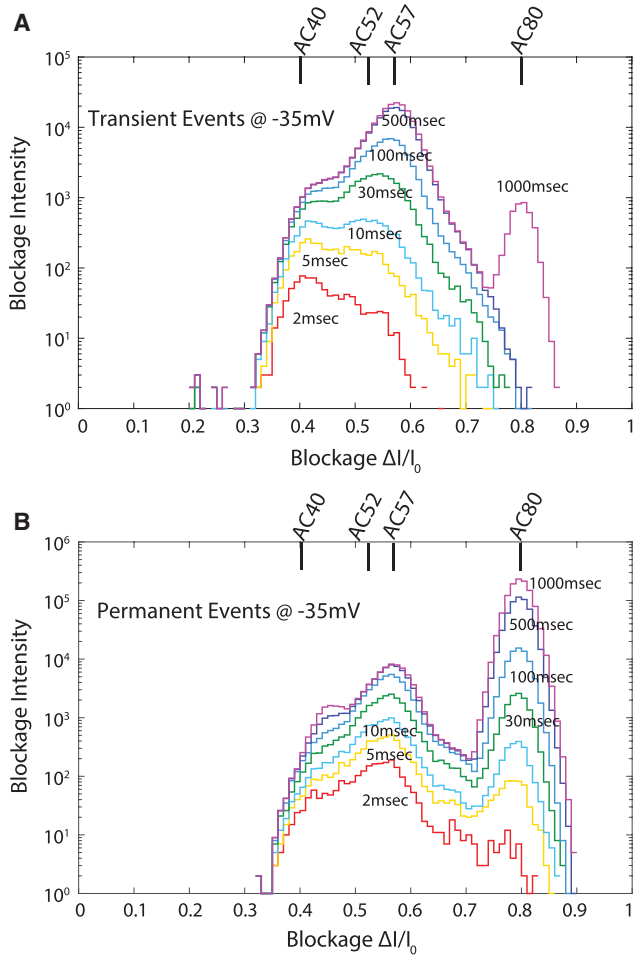

FIGURE 3 Protein dynamics landscape (PDL) plots. (*A*) Transient events are shown. Individual current blockage spectra are first obtained by grouping together all transient events that last for less than a given time, τ_{trans}, and then generating a histogram of the total amount of time spent (in units of 160 μs time bins) at each blockage level. Then the PDL plot is generated from a whole set of such histograms of level populations, obtained by varying the value τ_{trans} from 2 to 1000 ms, as indicated in the figure. (*B*) Permanent events are shown. Here all (205) permanent events are grouped, and each histogram refers to the number of times a blockage level appears up until a time τ_{perm} after the capture events start. The plot is generated from a set of histograms with τ_{perm} varying from 2 to 1000 ms. For both plots, the voltage is fixed at −35 mV. At the top of each PDL plot, we show discrete blockage levels that are deduced directly from the blockage peak positions in these plots by nonlinear least-squares fitting with sums of Gaussians, as described in the Supporting Materials and Methods. We denote the levels AC40, AC52, AC57, and AC80 as they correspond to avidin capture states with 40, 52, 57, and 80% current blockage, respectively. In addition to these levels, the fits reveal a fifth discrete blockage level at 45% current blockage.

The PDL here is obtained for a fixed bias voltage of −35 mV. The PDL plot reveals several peaks, corresponding to discrete blockage levels for avidin in ClyA. Note that deeper blockage levels last longer than shallower levels.

A similar analysis can be performed on permanent capture events, and the results are shown in Fig. 3 *B* for the same bias voltage of −35 mV. Here, all permanent capture events are considered together and each histogram refers to the accumulated time (in units of 160 μs) a blockage value appears up until τ_{perm} after a capture event starts (which is when avidin first enters the pore). The deepest-blockage level is maximally populated for the largest τ_{perm}.

A complete set of PDL plots is obtained from data like those of Fig. 3, *A* and *B* at different bias voltages and are shown in Fig. S2.

In the PDL plot of Fig. 3 *A*, we see a single peak centered at 40% blockage for transient events lasting 2 ms or less. We call this level AC40 (AC for "avidin capture"). As longer events are included (i.e., as τ_{trans} is increased), a second peak emerges. With careful fitting, we determine this level to be centered at 52% blockage and denote the level AC52. At 10 ms the two peaks have equal intensity, and at 30 ms, the AC52 peak dominates. For longer times, a separate (AC57) peak at 57% blockage dominates, and finally we observe a few very deep captures for transient events that last longer than 500 ms. Here the blockage level at 80% dominates (AC80). Gaussian fits to the spectra clearly reveal a fifth peak at 45% blockage (AC45), and the fits are shown in Fig. S3.

It is interesting to compare this dynamical behavior to that revealed by the PDL plot for permanent events at −35 mV (Fig. 3 *B*). During the first 2 ms of the permanent events, the spectrum is dominated by one peak: AC57. The AC40 peak is barely visible, and AC52 is missing. The spectra are generally dominated by AC57 during the early times of the permanent events, but later ($\geq$100 ms) the AC80 peak dominates. So for the permanently trapped events, avidin is first captured into state AC57, where it stays for an average of 60 ms (at −35 mV). This is followed by capture into a deeply and permanently trapped state, AC80. This picture is supported by the time traces for the Permanent Capture events in Fig. 2, *F* and *G*.

This difference between the peak-structure dynamics in the PDL plots for transient and permanent events—in particular the absence of the low-blockage peaks AC40, AC45, and AC52 in the PDL plot for permanent events—indicates that for avidin to reach the permanent trap state AC80, it has to enter the pore in a particular orientation. To illustrate, we show in Fig. 4 *A* a 3D printed macroscopic model of avidin (*black*) in a $ClyA_{12}$ pore (*red*) (the pore is partially cut out to aid in visualization). For the particular orientation of avidin relative to ClyA, shown in Fig. 4 *B*, there is a snug fit between the two and avidin can be deeply inserted in the form-fitting pore. (This orientation corresponds to the bottom avidin figure in Fig. 1 *B*.) We posit that the configuration shown here corresponds to the 57% blockage level AC57. In addition, ClyA is known to have a ring of negatively charged amino acids within the small aperture at the trans side (14,15,20). These nearby charges pull the trapped, positively charged avidin further into the pore and result in the stably trapped state with 80% blockage (AC80).

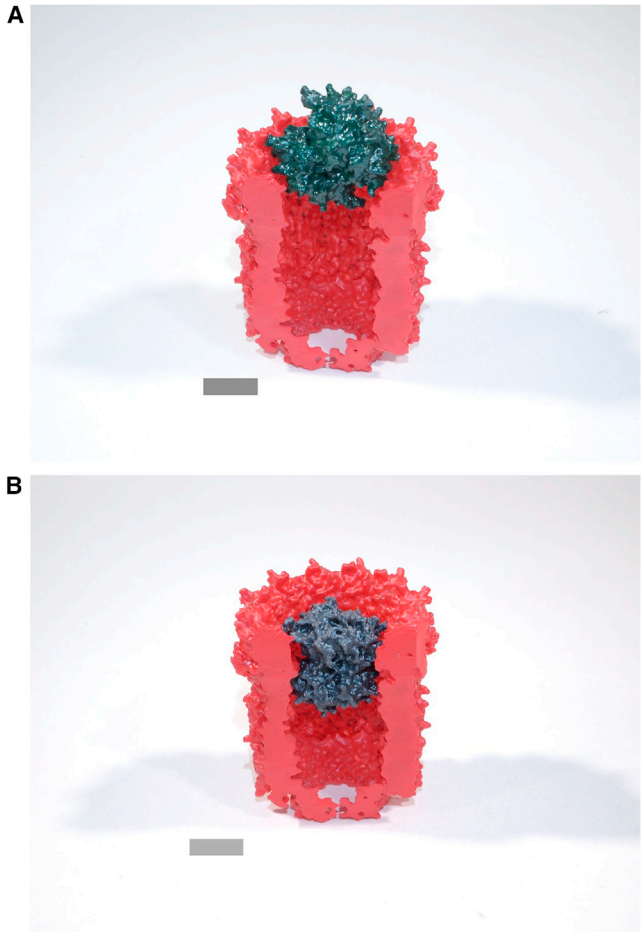

FIGURE 4 Avidin trapped in $ClyA_{12}$. We show a three-dimensional printed macroscopic model of avidin (*black*) in a $ClyA_{12}$ pore (*red*). The pore is partially cut out to aid in visualization. (*A*) Orientation of avidin that does not allow for entry into the pore is shown. (*B*) An orientation of avidin that allows it to be deeply inserted in the form-fitting pore leading to the deeply trapped state.

We also observe that the level populations in the PDLs are strongly voltage-bias-dependent (Fig. S2). This effect is already dramatically seen by simply plotting the ratio of the number of permanent to transient events as a function of bias voltage. This is shown in Fig. 5. Increasing the bias voltage from 30 to 50 mV results in dramatic and exponential increase in this ratio. At high bias voltage, the energy landscape of the protein in the pore is clearly biased toward permanently capturing the avidin to the deepest level in the pore from which escape eventually becomes impossible.

Biotin-avidin complex in a 1.66 nS pore

Finally and importantly, we have demonstrated the sensitivity of the avidin-ClyA platform for detecting other molecules attached to avidin. Here 100 pmol of biotin were

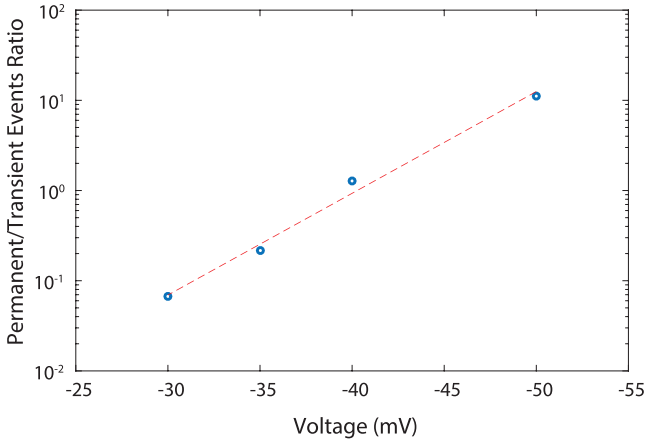

FIGURE 5 Ratio of the number of permanent to escape events as a function of voltage. The total event rate (transient and permanent) is 91 events/s at −30 mV and 176 events/s at −50 mV. To see this figure in color, go online.

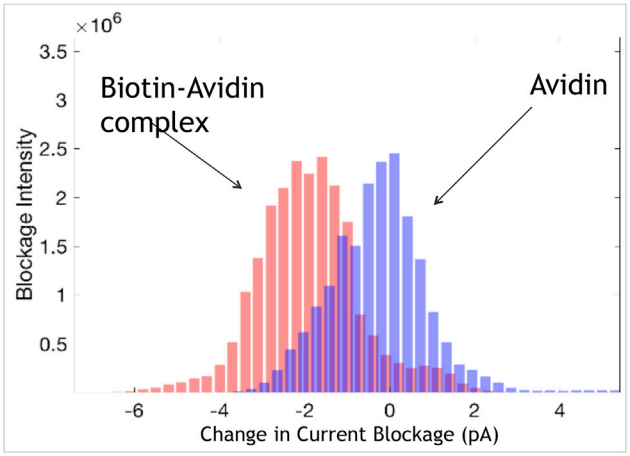

FIGURE 6 Biotin-avidin complex. Current-blockage spectra for the deeply trapped state for both the biotin-avidin complex and for avidin alone in a $ClyA_{12}$ nanopore biased at −35 mV are shown. The "change in current blockage" is the current blockage referenced to the peak current blockage for avidin in the permanent trap state. The unit for the vertical axis is 4 μs. A 100-point median filter has been applied to the raw data sampled every 4 μs.

added to the *cis* chamber already containing 10 pmol of avidin at −35 mV voltage bias. After a few minutes, we observed a dramatic change in the trapping dynamics. The ratio of permanent to transient event rates was reduced by a factor of 28, from 1/6.4 (avidin) to 1/182 (biotin-avidin), with the latter closely resembling the ratio for avidin alone at −30 mV bias voltage (1/159). From this we conclude that the net positive charge of the biotin-avidin complex is lower by a factor of 30/35 compared to avidin alone. Calculations (19) based on the protein data bank crystallographic structures for deglycosylated avidin (1AVE) and for the complex of deglycosylated avidin with four biotin ligands (2AVI) predict a charge of the biotin-avidin complex that is lower by two positive charge units than that of avidin alone. (Note, in both these cases avidin is deglycosylated except for the core glucosamine (GlcNAc)). Combining this with our observations, we obtain a charge of +14e for fully glycosylated avidin (used in our experiments).

Interestingly, we also observe that for the biotin-avidin complex, the blockage level for the deeply trapped state is decreased by 4% relative to that for avidin alone. This is shown in Fig. 6. Since the deep blockage level for avidin is independent of voltage in the −30 to −35 mV range, the difference in deep blockage levels could be due to a slightly bigger size or lower elasticity of the biotin-avidin complex (12,21). An alternative explanation is a weaker electrostatic attraction of biotin-avidin to the negative charges at the limiting aperture of ClyA.

CONCLUSIONS

Our experiments and analysis show that the avidin-ClyA nanopore system can be electronically probed and quantified in great detail. Discrete conductance levels, transitions between them, and the fluctuations within them all reflect the interaction between, and time evolution of, avidin and the voltage-biased pore in an electrolyte environment. One may expect that the discussions we have presented will be made more precise when the powerful computational tools of molecular modeling and simulation of ionic conduction in confined spaces are applied to this system (22). An important motivation for focusing on the avidin-ClyA system is the potential it presents for using avidin as a shuttle to bring other, biotinylated biological molecules linked to avidin to the pore for probing. Here, the deeply trapped state will be of special importance, allowing for probing at the single-molecule level over controllable time intervals against a low-noise background. A first step in this direction has already been taken by our detection of biotin attached to deeply captured avidin.

SUPPORTING MATERIAL

Supporting Materials and Methods, three figures, and three tables are available at http://www.biophysj.org/biophysj/supplemental/S0006-3495(18)30910-X.

AUTHOR CONTRIBUTIONS

B.L. contributed experimental work and computing assistance at Harvard. C.S. prepared three-dimensional protein models and performed experiments at Harvard. M.F. prepared ClyA at Amherst. M.C. directed work on expression and purification of ClyA at Amherst. J.A.G. and L.V.H. conceived the idea for the experiment and method of analysis, and directed research at Harvard, and in addition L.V.H. conducted experiments at Harvard.

ACKNOWLEDGMENTS

We thank Eric Brandin for biochemical preparations and evaluations and Stephen Fleming for assistance and advice.

REFERENCES

1. Deamer, D., M. Akeson, and D. Branton. 2016. Three decades of nanopore sequencing. *Nat. Biotechnol.* 34:518–524.
2. Fologea, D., B. Ledden, …, J. Li. 2007. Electrical characterization of protein molecules by a solid-state nanopore. *Appl. Phys. Lett.* 91:539011–539013.
3. Yusko, E. C., J. M. Johnson, …, M. Mayer. 2011. Controlling protein translocation through nanopores with bio-inspired fluid walls. *Nat. Nanotechnol.* 6:253–260.
4. Japrung, D., J. Dogan, …, J. B. Edel. 2013. Single-molecule studies of intrinsically disordered proteins using solid-state nanopores. *Anal. Chem.* 85:2449–2456.
5. Nivala, J., D. B. Marks, and M. Akeson. 2013. Unfoldase-mediated protein translocation through an α-hemolysin nanopore. *Nat. Biotechnol.* 31:247–250.
6. Rosen, C. B., D. Rodriguez-Larrea, and H. Bayley. 2014. Single-molecule site-specific detection of protein phosphorylation with a nanopore. *Nat. Biotechnol.* 32:179–181.
7. Wu, D., S. Bi, …, J. Yang. 2014. Single-molecule study of proteins by biological nanopore sensors. *Sensors (Basel).* 14:18211–18222.
8. Soskine, M., A. Biesemans, …, G. Maglia. 2012. An engineered ClyA nanopore detects folded target proteins by selective external association and pore entry. *Nano Lett.* 12:4895–4900.
9. Wloka, C., V. Van Meervelt, …, G. Maglia. 2017. Label-free and real-time detection of protein ubiquitination with a biological nanopore. *ACS Nano.* 11:4387–4394.
10. Green, N. M. 1975. Avidin. *Adv. Protein Chem.* 29:85–133.
11. Bruch, R. C., and H. B. I. White, 3rd. 1982. Compositional and structural heterogeneity of avidin glycopeptides. *Biochemistry.* 21:5334–5341.
12. Livnah, O., E. A. Bayer, …, J. L. Sussman. 1993. Three-dimensional structures of avidin and the avidin-biotin complex. *Proc. Natl. Acad. Sci. USA.* 90:5076–5080.
13. Pugliese, L., M. Malcovati, …, M. Bolognesi. 1994. Crystal structure of apo-avidin from hen egg-white. *J. Mol. Biol.* 235:42–46.
14. Soskine, M., A. Biesemans, …, G. Maglia. 2013. Tuning the size and properties of ClyA nanopores assisted by directed evolution. *J. Am. Chem. Soc.* 135:13456–13463.
15. Mueller, M., U. Grauschopf, …, N. Ban. 2009. The structure of a cytolytic alpha-helical toxin pore reveals its assembly mechanism. *Nature.* 459:726–730.
16. Berman, H. M., J. Westbrook, …, P. E. Bourne. 2000. The protein data bank. *Nucleic Acids Res.* 28:235–242.
17. Benke, S., D. Roderer, …, B. Schuler. 2015. The assembly dynamics of the cytolytic pore toxin ClyA. *Nat. Commun.* 6:6198.
18. Wilchek, M., and E. Bayer. 1990. Avidin-Biotin TechnologyVolume 184. Academic Press, Cambridge, MA.
19. Dolinsky, T. J., J. E. Nielsen, …, N. A. Baker. 2004. PDB2PQR: an automated pipeline for the setup of Poisson-Boltzmann electrostatics calculations. *Nucleic Acids Res.* 32:W665–W667.
20. Ludwig, A., S. Bauer, …, W. Goebel. 1999. Analysis of the SlyA-controlled expression, subcellular localization and pore-forming activity of a 34 kDa haemolysin (ClyA) from *Escherichia coli* K-12. *Mol. Microbiol.* 31:557–567.
21. Celej, M. S., G. G. Montich, and G. D. Fidelio. 2004. Conformational flexibility of avidin: the influence of biotin binding. *Biochem. Biophys. Res. Commun.* 325:922–927.
22. Maffeo, C., S. Bhattacharya, …, A. Aksimentiev. 2012. Modeling and simulation of ion channels. *Chem. Rev.* 112:6250–6284.

Biophysical Journal, Volume *115*

Supplemental Information

Protein Motion and Configurations in a Form-Fitting Nanopore: Avidin in ClyA

Bo Lu, Chris Stokes, Monifa Fahie, Min Chen, Jene A. Golovchenko, and Lene Vestergaard Hau

Supporting Material

Protein Motion and Configurations in a Form-Fitting Nanopore: Avidin in ClyA

B. Lu, C. Stokes, M. Fahie, M. Chen, J.A. Golovchenko, and L.V. Hau

Scatter Plots for Different Bias Voltages.

The scatter plot for a bias voltage of -35 mV is shown in the main text (Fig. 2h). In Figure S1 we show scatter plots for bias voltages of -50 mV, -40 mV, and -30 mV.

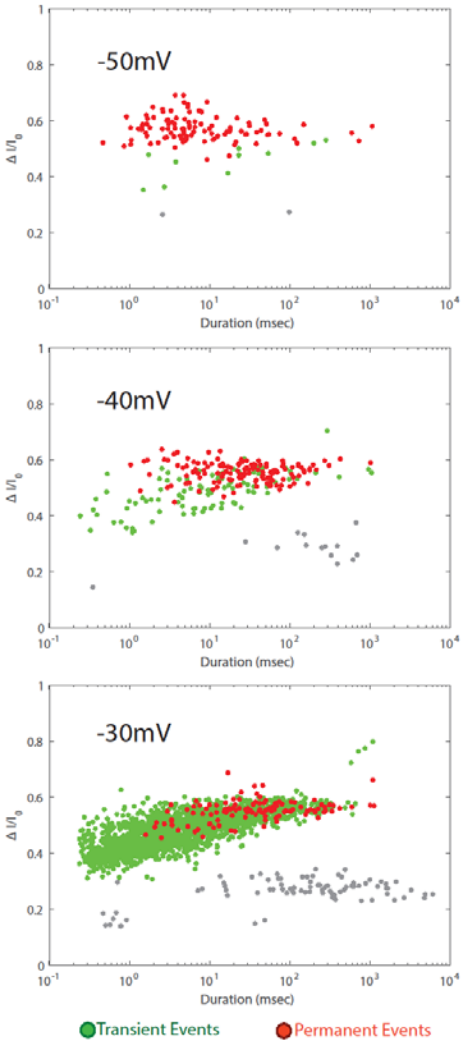

Figure S1: Scatter plots for Transient and Permanent Capture Events for bias voltages of -50 mV, -40 mV and -30 mV.

PDL Plots for Different Bias Voltages.

The PDL plots for Transient and Permanent Captures are shown in the main text for -35 mV. In Figure S2 we show PDL plots for bias voltages of -40 mV (**A**) and -30 mV (**B**). Fitting parameters for the plots are indicated in tables below the figures.

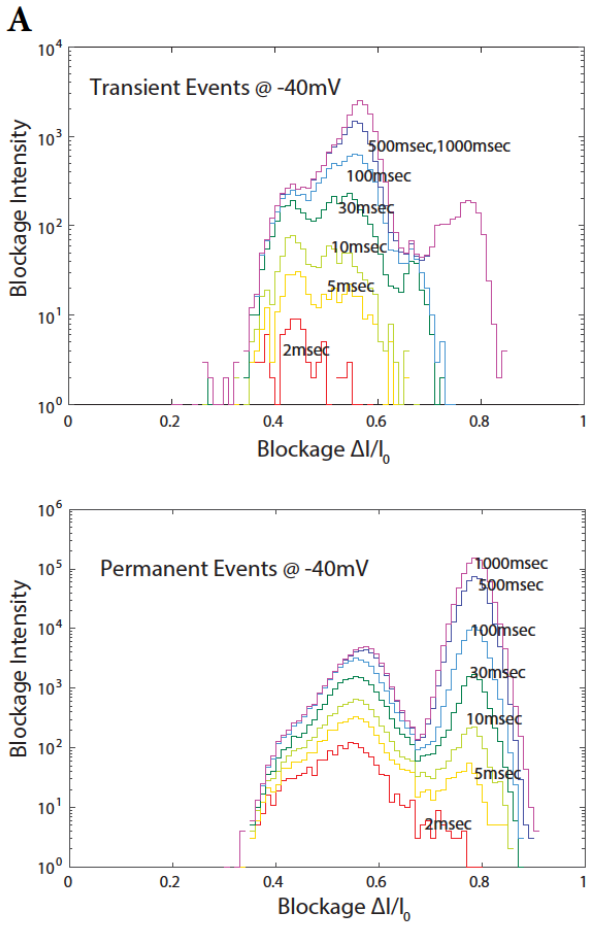

Figure S2 (A): PDL plots for transient and permanent captures for voltage -40 mV. Table S1 (below) shows the number of transient events for each blockage spectrum in the PDL plot for transient events. Also listed is the number of permanent events in the PDL plot for these events.

Table S1

τ_{trans}	2ms	5ms	10ms	30ms	100ms	500ms	1000ms
Number of transient events	20	35	48	73	88	93	94

Total number of permanent events at -40mV is 139.

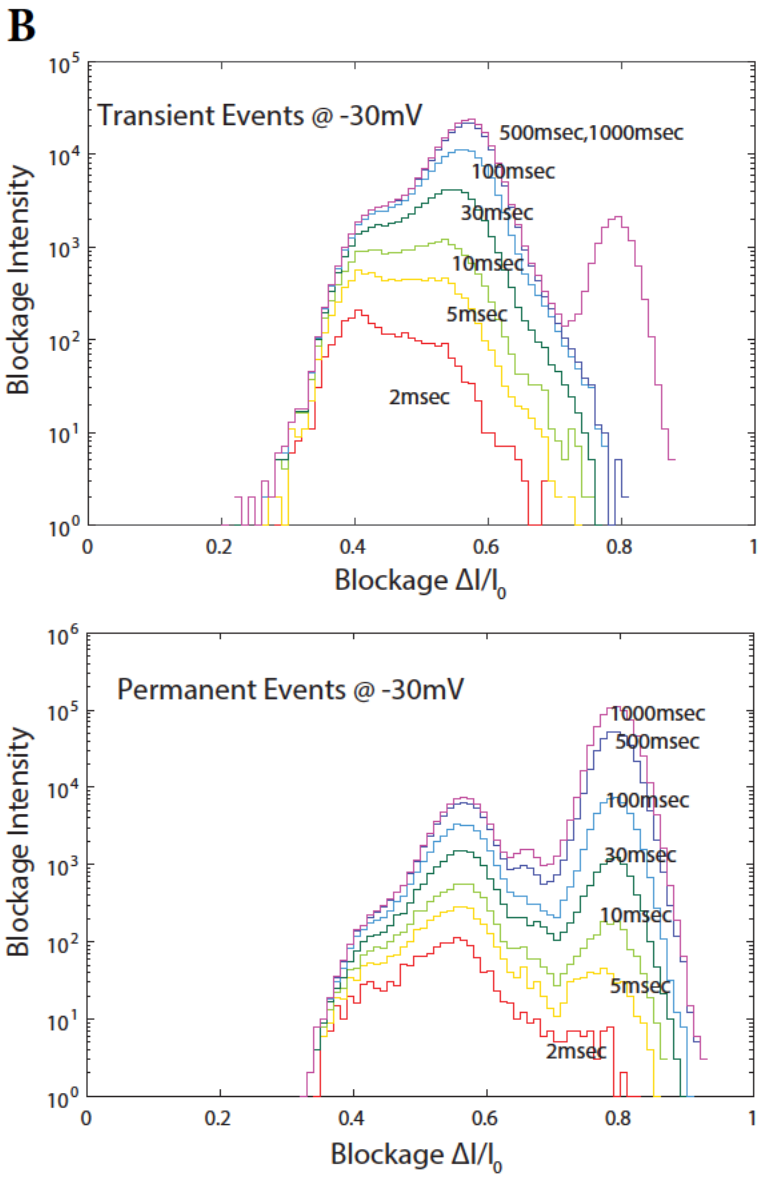

Figure S2 (B): PDL plots for transient and permanent captures for voltage -30 mV. Table S2 (below) shows the number of transient events for each blockage spectrum in the PDL plot for transient events. Also listed is the number of permanent events in the PDL plot for these events.

Table S2

τ_{trans}	2ms	5ms	10ms	30ms	100ms	500ms	1000ms
Number of transient events	566	943	1205	1552	1781	1854	1861

Total number of permanent events at -30mV is 131.

Determination of Blockage Levels AC40, AC45, AC52, and AC57.

The positions of discrete blockage levels are obtained from fits to blockage spectra in a PDL plot. For the PDL plot for transient events at -35 mV (Fig. 3a in the main text), we obtain the levels below the 80% permanent level (AC80) by fitting a sum of four Gaussians to each spectrum for blockages below 65%.

For efficient convergence of the fitting routine, we use the following procedure:

First the spectrum for τ_{trans} = 1000ms is considered. We fit one Gaussian to the spectrum in a restricted blockage region around the dominant 57% peak, and then subtract the resulting Gaussian from the data. The result of this subtraction shows the 52% peak clearly and we fit with a single Gaussian in a blockage region around that peak and again subtract the resulting Gaussian. This reveals the 45% peak which is fitted with a Gaussian in a restricted blockage region. The resulting values for the position and width of the two Gaussians centered at 57% (AC57) and 45% (AC45) are then used as fixed values for fits with four Gaussians to all spectra over the whole blockage region below 65%. The result of the fits and the values of positions, widths, and amplitudes of each Gaussian component are shown in Fig. S3.

Figure S3: (see below) Gaussian fits to the PDL blockage spectra at -35 mV. The data (red dots), fit function (solid blue curve), and the four individual Gaussians are shown for each blockage spectrum, with τ_{trans} indicated in Figures S3, A-G.

The results of the fitting procedure for the position (Pos), width (Sigma), and amplitude (Amp) of each peak and for each spectrum are shown in Table S3, below. The table is below all the plots.

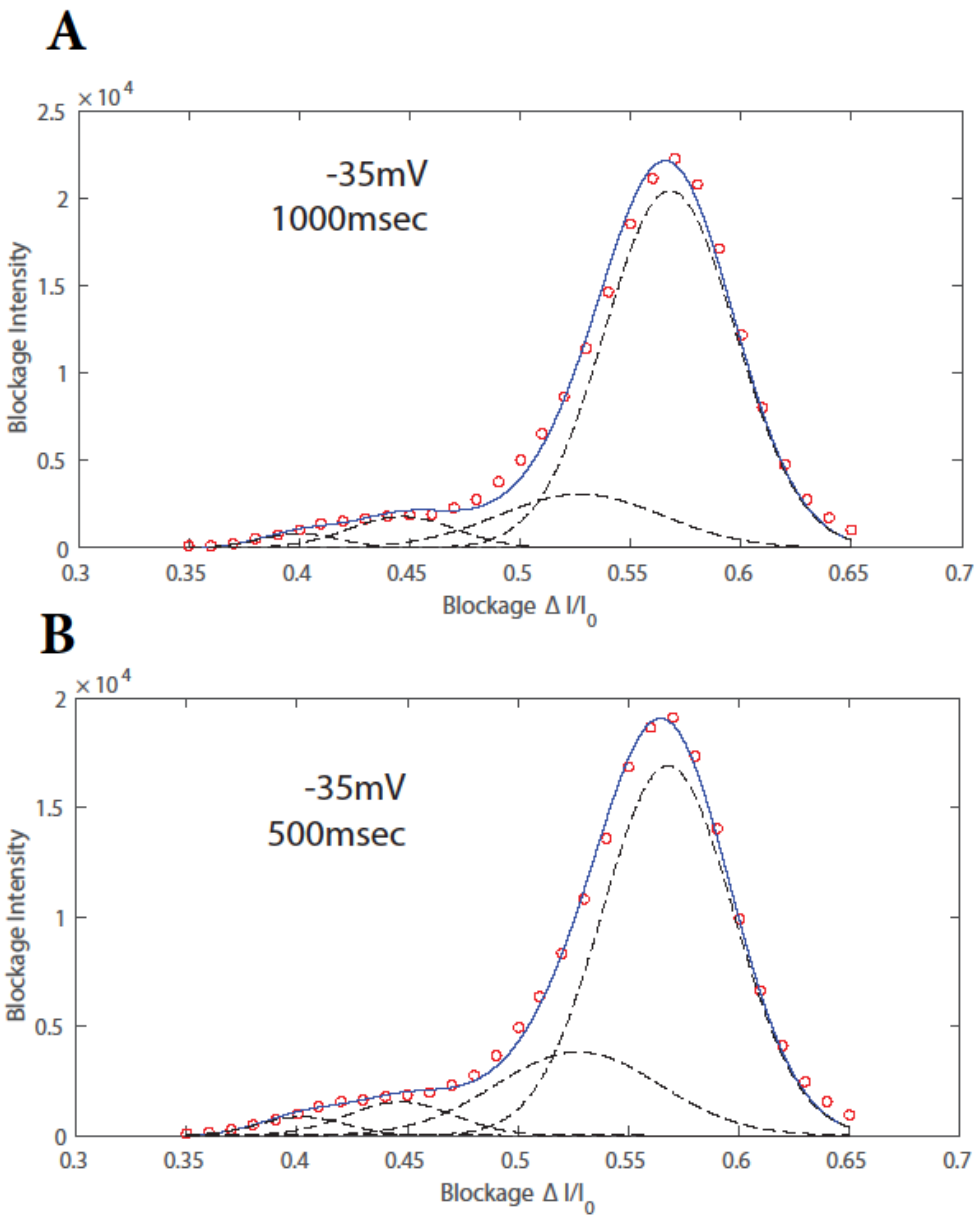
A
× 10^4
2.5
2
1.5
1
0.5
0
-35mV
1000msec
Blockage Intensity
0.3
0.35
0.4
0.45
0.5
0.55
0.6
0.65
0.7
Blockage Δ I/I0
B
× 10^4
2
1.5
1
0.5
0
-35mV
500msec
Blockage Intensity
0.3
0.35
0.4
0.45
0.5
0.55
0.6
0.65
0.7
Blockage Δ I/I0

Figure S3

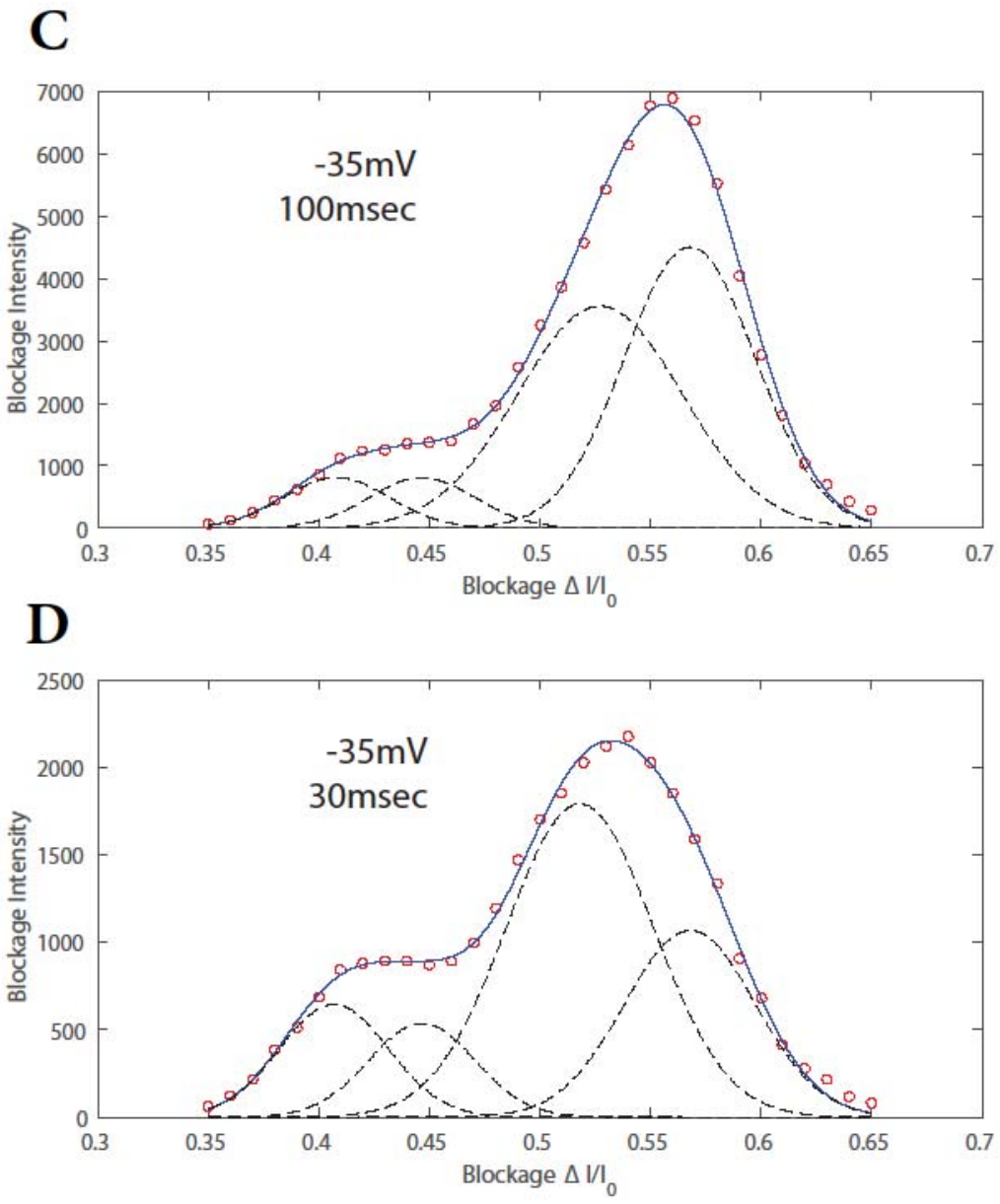
C
-35mV
100msec
Blockage Intensity
Blockage Δ I/I0
D
-35mV
30msec
Blockage Intensity
Blockage Δ I/I0

Figure S3

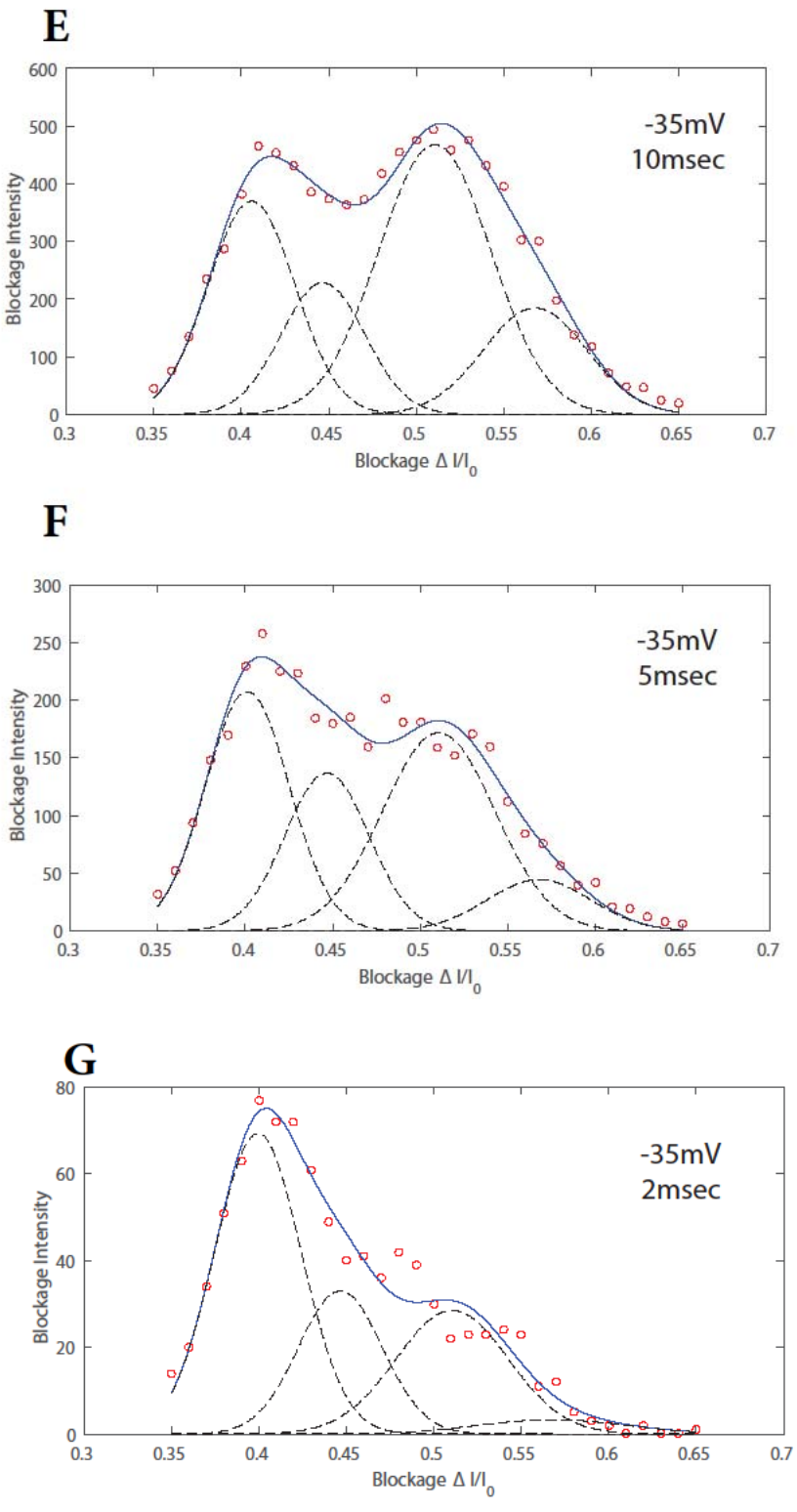
E
-35mV
10msec
Blockage Intensity
Blockage Δ I/I0
F
-35mV
5msec
Blockage Intensity
Blockage Δ I/I0
G
-35mV
2msec
Blockage Intensity
Blockage Δ I/I0

Figure S3

Table S3

τ_{trans}	AC40			AC45	AC52			AC57
	Amp	Pos	Sigma	Amp	Amp	Pos	Sigma	Amp
1000	817 ±434	0.4001 ±0.0123	0.0178 ±0.0125	1792 ±411	3068 ±351	0.5272	0.0371	20422 ±373
500	847 ±251	0.4024 ±0.0081	0.0194 ±0.0081	1531 ±285	3818 ±213	0.5272	0.0371	16914 ±232
100	809 ±78	0.4080 ±0.0047	0.0240 ±0.004	808 ±165	3561 ±69	0.5272	0.0371	4506 ±74
30	644 ±28	0.4069 ±0.0022	0.0247 ±0.0019	537 ±61	1793 ±23	0.5181	0.0333	1069 ±23
10	370 ±12	0.4058 ±0.0017	0.0248 ±0.0015	228 ±27	468 ±10	0.5106	0.0321	185 ±10
5	207 ±9	0.4012 ±0.0018	0.0240 ±0.0018	136 ±15	172 ±8	0.5106	0.0321	44 ±7
2	69 ±3	0.3996 ±0.0016	0.0248 ±0.0016	33 ±5	29 ±2	0.5106	0.0321	3 ±2

AC45 Pos = 0.4501 ±0.002, AC45 Sigma=0.0252 ±0.002
AC57 Pos = 0.5679 ±0.001, AC57 Sigma=0.0296 ±0.001